Pericentromere tension is self-regulated by spindle structure in metaphase

Jeremy M. Chacón, Soumya Mukherjee, Breanna M. Schuster, Duncan J. Clarke, and Melissa K. Gardner

Department of Genetics, Cell Biology, and Development, University of Minnesota, Minneapolis, MN 55455

During cell division, a mitotic spindle is built by the cell and acts to align and stretch duplicated sister chromosomes before their ultimate segregation into daughter cells. Stretching of the pericentromeric chromatin during metaphase is thought to generate a tension-based signal that promotes proper chromosome segregation. However, it is not known whether the mitotic spindle actively maintains a set point tension magnitude for properly attached sister chromosomes to facilitate robust mechanochemical checkpoint signaling. By imaging and tracking the thermal movements of pericentromeric fluorescent markers in *Saccharomyces cerevisiae*, we measured pericentromere stiffness and then used the stiffness measurements to quantitatively evaluate the tension generated by pericentromere stretch during metaphase in wild-type cells and in mutants with disrupted chromosome structure. We found that pericentromere tension in yeast is substantial (4–6 pN) and is tightly self-regulated by the mitotic spindle: through adjustments in spindle structure, the cell maintains wild-type tension magnitudes even when pericentromere stiffness is disrupted.

Introduction

During mitosis, microtubules and motors generate forces to align and stretch duplicated sister chromatids along the spindle axis, leading to tension (Dumont and Mitchison, 2009). This tension is applied at the pericentromere, which includes the chromatin and interchromosomal linkages near to the centromeres (Fig. 1 A). It is thought that the spindle assembly checkpoint may sense tension to detect erroneous kinetochore microtubule (kMT) attachments (Bakhoum et al., 2009; Khodjakov and Pines, 2010; Thompson et al., 2010). However, it is not known whether the mitotic spindle acts to maintain a set point tension magnitude to facilitate robust mechanochemical checkpoint signaling during metaphase.

In the work described here, we used an imaging-based approach to make quantitative estimates of pericentromere stiffness. These estimates were then used to evaluate pericentromere tension in wild-type (WT) cells and in mutant cells with disrupted pericentromere structure (Fig. 1 A, $F_{tension}$). We found that pericentromere tension in yeast is substantial (4–6 pN) and is tightly self-regulated by the mitotic spindle: the cell maintains WT tension magnitudes even when the pericentromere stiffness is disrupted. Our results suggest that maintenance of a metaphase tension set point may be an important characteristic of mitosis.

Results and discussion

In vivo characterization of pericentromere stiffness in yeast

To characterize pericentromere tension, it was first necessary to quantitatively characterize pericentromere stiffness. We measured stiffness by tracking the movements of pericentromeric fluorescent tags that occur as a result of thermal energy in the cell (Alexander and Rieder, 1991; Mickey and Howard, 1995; Marshall et al., 1997, 2001; Poirier et al., 2002; Levi et al., 2005). Here, thermally driven movements of a fluorescent pericentromeric tag will be large if the pericentromere is soft, whereas stiffer pericentromeres will lead to smaller displacements of the pericentromeric tag over time (Video 1).

This general principle, in which the thermal movements of a fluorescent spot on a constrained polymer such as DNA reflect the stiffness of the polymer itself, is quantitatively described by the equipartition theorem, which relates the thermal

Correspondence to Melissa K. Gardner: klei0091@umn.edu

Abbreviations used in this paper: fps, frame per second; kMT, kinetochore microtubule; MSD, mean-squared displacement; SD, synthetic designed; TIRF, total internal reflection fluorescence; WT, wild type.

The Rockefeller University Press $30.00
J. Cell Biol. Vol. 205 No. 3 313–324
www.jcb.org/cgi/doi/10.1083/jcb.201312024

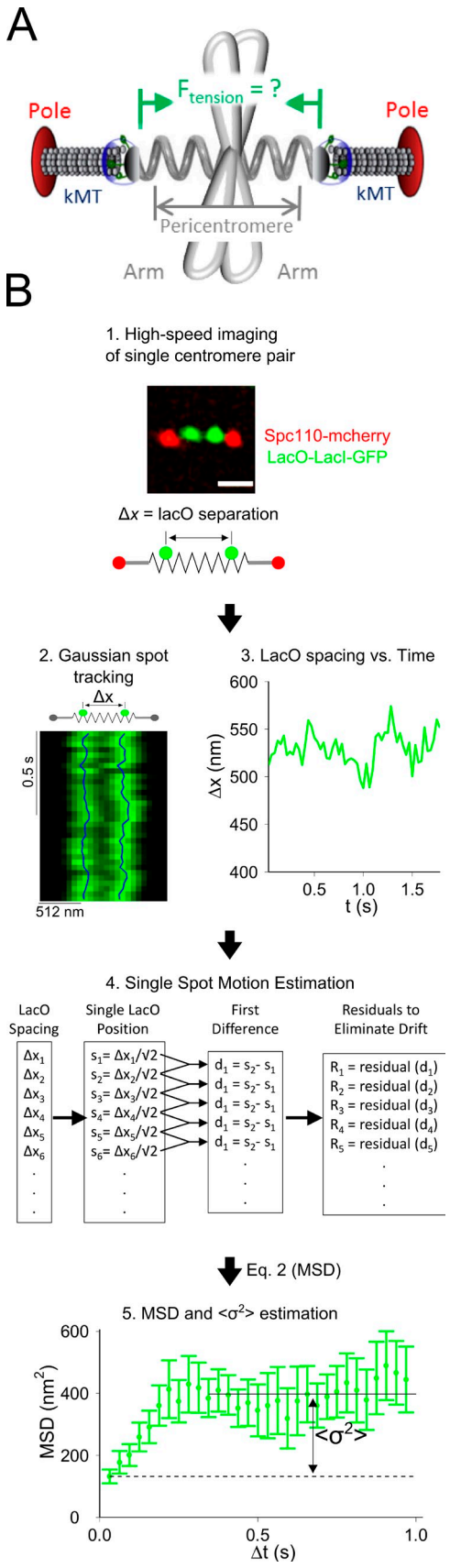

Figure 1. **In vivo pericentromere stiffness measurement.** (A) Cartoon of yeast metaphase spindle denoting pericentromere location and tension. (B, 1) Gaussian-filtered experimental yeast metaphase spindle with fluorescent tags: LacO/lacI-GFP (lacO spots) and Spc110-mCherry (poles). Bar, 1 µm. (2) lacO spots were tracked using Gaussian mixture model fitting (blue lines). (3) The distance between the lacO spots (Δx_i) over time. (4) Estimation of single spot motion and drift correction. (5) Eq. 2 converts R_i values to MSD, and then, the maximum motion ($<\sigma^2>$) is estimated. Error bars = SEMs.

energy (in k_BT) to the maximum mean-squared displacement (MSD) of the fluorescent pericentromeric tag:

$$\kappa = \frac{k_B T}{<\sigma^2>}. \quad (1)$$

Here, κ is the spring constant, which in our assay represents the stiffness of the metaphase pericentromere, k_B is Boltzmann's constant, T is the absolute temperature (in Kelvin), and $<\sigma^2>$ is the maximum MSD of the pericentromeric tag (Svoboda et al., 1993; Mickey and Howard, 1995; Kamiti and van De Ven, 1996; Bustamante et al., 2000).

We applied this approach in budding yeast metaphase spindles (*Saccharomyces cerevisiae*), by using a lacI (lac repressor)-GFP–expressing strain with 33 lacO (lac operon) repeats inserted 1.1 kb 3′ to *CEN*3 (Pearson et al., 2001). During metaphase in budding yeast, the pericentromeric lacO/lacI-GFP arrays are readily apparent as two separated spots, which we will refer to as lacO spots (Fig. 1 B, 1, green). In addition, red Spc110-mCherry–labeled spindle poles were used to specifically select in-plane metaphase mitotic spindles for analysis (Fig. 1 B, 1, red).

The movements of the green lacO spots were observed by collecting time-lapse videos of metaphase spindles (Fig. 1 B, 2). However, the movements of the lacO spots can only be used to quantitatively assess pericentromere stiffness (κ) if the lacO spot movements are caused by thermal energy alone: movements of the lacO spots that originate from kMT dynamics or from ATP-driven motor forces do not quantitatively reflect pericentromere stiffness. This is because the equipartition theorem (Eq. 1) relates lacO spot movements to pericentromere stiffness (κ) through the factor k_BT, which exclusively represents the thermal energy available in the cell. Therefore, to stabilize kMT and motor-driven dynamics over the time scale of the experiment, cells were treated with stabilizing drugs (azide ± deoxyglucose or low-dose benomyl), and/or rapid time-lapse videos were collected (32 frames per second [fps] and 48 fps). We predicted that even without the drug treatments, the movements of the lacO spots in the 32 and 48 fps videos would reflect thermal fluctuations because movements originating from yeast kMT dynamics and/or motors occur on a much slower time scale than would be apparent using this rapid frame rate (see Materials and methods; Maddox et al., 2000; Sprague et al., 2003; Gupta et al., 2006; Pearson et al., 2006).

Iterative Gaussian mixture model fitting was then used to track the distance between the lacO spots along the spindle axis with subpixel resolution (Δx; Thomann et al., 2002; Jaqaman et al., 2008), leading to a list of Δx_i values corresponding to increasing time points in each video (Fig. 1 B, 2 and 3). To estimate the displacements of a single lacO spot, (a) Δx_i values were divided by $\sqrt{2}$ (i.e., $s_i = \Delta x_i/\sqrt{2}$), which is equivalent to halving the

MSDs for the distance between two independently moving lacO spots (Fig. S1 A); (b) first differences were calculated (d_i); and (c) d_i values were converted to drift-corrected residuals (R_i; Fig. 1 B, 4). Finally, MSDs were calculated for increasing time intervals (Δt) according to

$$\mathrm{MSD}(\Delta t) = \frac{1}{n}\sum_{j=1}^{n}\left(\sum_{i=j}^{j+(\Delta t/t_{step})-1} R_i\right)^2. \quad (2)$$

Here, t_{step} is the time step size between image frames in the movies, and n is the number of displacements (Michalet, 2010). The MSD values were then plotted for increasing time intervals (Δt; Fig. 1 B, 5). As is expected for constrained diffusion, the plots of MSD versus Δt reached a plateau (Fig. 2 A; Howard, 2001). Using these plots, the maximum MSD value ($\langle\sigma^2\rangle$) was calculated as $\langle\sigma^2\rangle = \mathrm{MSD}_{plateau} - \mathrm{MSD}(\Delta t_1)$. To calculate pericentromere stiffness, $\langle\sigma^2\rangle$ was then substituted into Eq. 1 (Fig. 2 B; see Materials and methods and Fig. S1 for details and extensive discussion of method validations).

The pericentromere stiffness estimates were statistically indistinguishable regardless of growth media, drug treatment, fast-imaging frame rate, or lacO spacing distance (at 32 fps: synthetic designed [SD] vs. azide, P = 0.18; H_2O vs. azide, P = 0.11; *t* test assuming unequal variances; Fig. 2 B and Fig. S1, F–H), which justified the use of live-cell (no drug) fast imaging for our subsequent stiffness measurements. The mean value over all treatments was 15.5 ± 1.3 pN/µm, which is on the order of previously reported chromosome stiffness values that were measured with micromanipulation techniques (decatenated newt mitotic chromosomes ~50 pN/µm; Kawamura et al., 2010) as well as similar to chromosome stiffness values estimated with viscoelasticity analysis after laser cutting of kMTs in *Schizosaccharomyces pombe* (~42 pN/µm; Gay et al., 2012). However, our metaphase value of κ = ~16 pN/µm is substantially higher than in a recent yeast interphase study, likely because the interphase values were measured using slow time-lapse imaging without drug treatments to stabilize active forces (Fig. S1, D and E; Verdaasdonk et al., 2013).

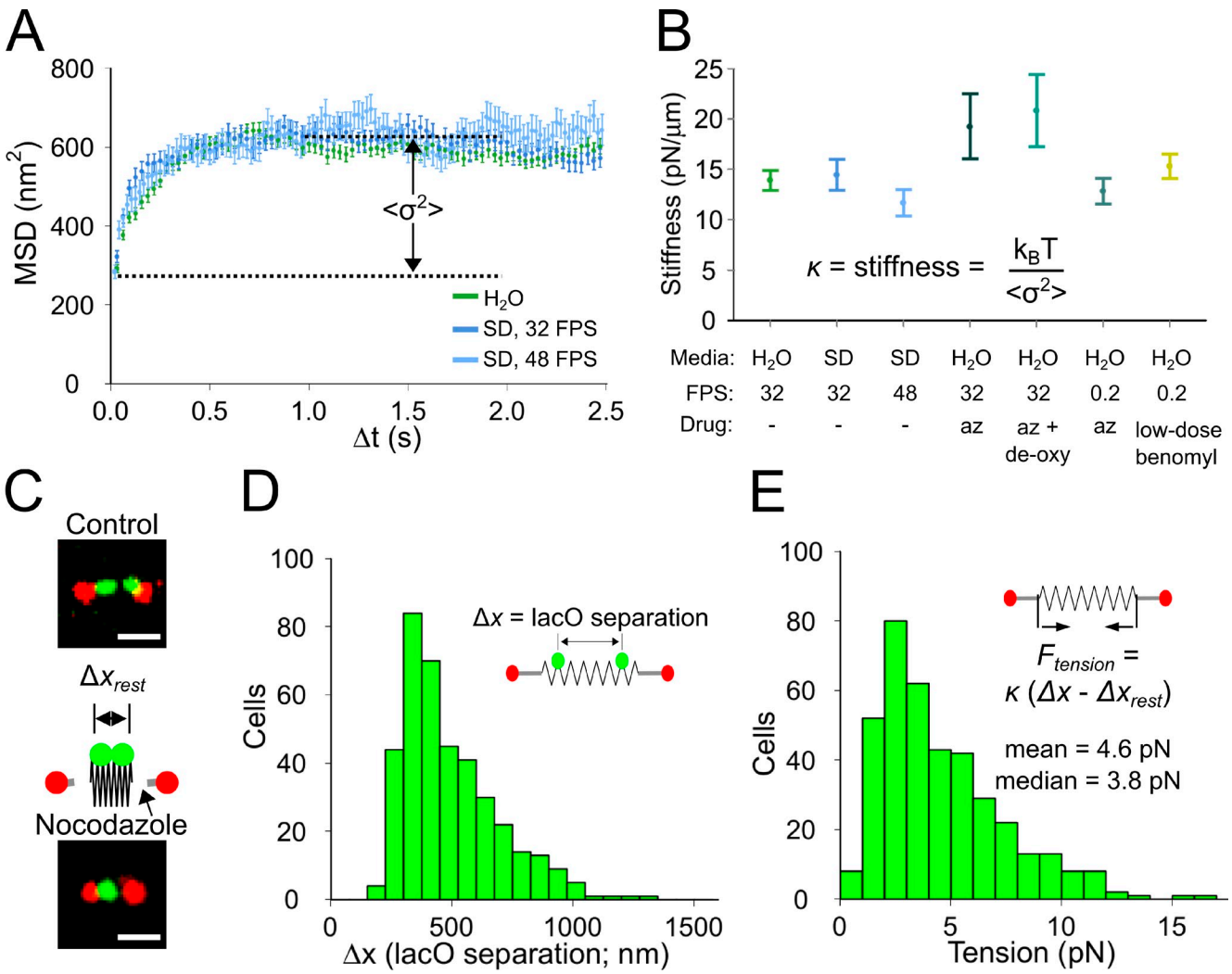

Figure 2. **Substantial pericentromere stretching tension in budding yeast metaphase.** (A) MSD versus time step size in WT cells (W303 strain background). (B) Mean pericentromere stiffness using different treatments. az = azide. (C) Estimating pericentromere rest length using nocodazole (see Materials and methods). Bars, 1 µm. (D) lacO spot separation distances in live cells (*n* = 390). (E) Pericentromere tension (*n* = 390). Error bars = SEMs.

In vivo metaphase pericentromere tension in budding yeast

We then used the pericentromere stiffness values (κ) to estimate in vivo pericentromere tension in budding yeast (Fig. 1 A, $F_{tension}$). This was performed by applying Hooke's law, which is

$$F_{tension} = \kappa\left(\Delta x - \Delta x_{rest}\right), \quad (3)$$

in which $F_{tension}$ is the pericentromere tension, Δx is the lacO spot separation distance, κ is the pericentromere stiffness, and Δx_{rest} is the "rest" separation distance between lacO spots when $F_{tension} = 0$ pN. To estimate Δx_{rest} for yeast, we treated cells with nocodazole, which depolymerizes kMTs and thus eliminates microtubule-associated pulling forces (see Materials and methods; Δx_{rest} = ∼170 nm; Fig. 2 C; Waters et al., 1996; Ribeiro et al., 2009). We measured the range of lacO spot separations (Δx) in live cells (n = 387 cells; Fig. 2 D) and then used these values to directly calculate the distribution of pericentromere tension (Fig. 2 E). We found that the pericentromere tension was 4.6 ± 0.1 pN in budding yeast (W303 strain background; mean ± SEM). This is nearly three orders of magnitude higher than is predicted for random thermal forces ($F_{thermal}$ = ∼0.01 pN; see Materials and methods), suggesting that pericentromere tension could provide an important mechanical signal during mitosis.

Similar previously published in vivo mitotic and meiotic force measurements are summarized in Table S1. Here, measured forces ranged from 0.2 to 75 pN/kMT, with a mean value over all observations of ∼16 pN/kMT. The measurement that is perhaps closest to our work was performed in meiotic grasshopper spermatocytes, in which pericentromere tension was evaluated by measuring the extent of chromosome elongation during prometaphase (Nicklas, 1988). Here, tension was measured as ∼7 pN/kMT, which is similar to our pericentromere tension value in yeast of ∼5 pN/kMT. We note that larger estimated forces were generally required to halt microtubule-mediated chromosome motion (Table S1), suggesting that the maximum kMT depolymerization force (Grishchuk et al., 2005; Volkov et al., 2013) may be substantially higher than the mean pericentromere tension. This may be because large inwardly directed tension could overpower Kinesin-5–mediated outwardly directed spindle forces, leading to spindle collapse and, ultimately, a drop in pericentromere tension (Bouck and Bloom, 2007).

Evidence for maintenance of a set point tension magnitude in yeast

Our results suggest that pericentromere tension could provide an important mechanical signal during metaphase. Therefore, it may be that the cell maintains a robust tension signal even in the presence of chromatin stiffness alterations, as could naturally occur as a result of stochastic variations in chromatin packaging (Moser and Swedlow, 2011). We tested this hypothesis using *top2-4* cells, which have altered chromatin structure (DiNardo et al., 1984; Warsi et al., 2008). Thus, we performed the MSD analysis in isogenic strain background WT and *top2-4* mutant cells (15D strain background; Fig. 3, A and B). We found that the WT 15D strain had a similar stiffness to the WT W303 strain ($\kappa_{WT,15D}$ = 14.2 ± 1.4 pN/µm and $\kappa_{WT,W303}$ = 13.9 ± 1.0 pN/µm; both H_2O at 32 fps). In contrast, pericentromeres in the mutant *top2-4* cells were nearly twofold less stiff than in WT cells ($\kappa_{top2\text{-}4}$ = 7.5 ± 0.7 pN/µm; Fig. 3 C).

We then calculated and compared pericentromere tension in WT and *top2-4* metaphase spindles. Here, Eq. 3 (Hooke's law) was used to calculate tension, which depends on both the stiffness (κ) as well as the net pericentromere stretch ($\Delta x - \Delta x_{rest}$), such that an increase in stretch could potentially compensate for softer stiffness to maintain tension. As was previously reported, we found that lacO spots were indeed farther apart in *top2-4* cells as compared with WT cells ($P < 0.001$, *t* test; Fig. 3 D). Importantly, because of the decreased *top2-4* stiffness, this corresponding increase in stretch resulted in tension magnitudes that were statistically indistinguishable between WT and *top2-4* cells ($F_{tension,\ WT\ 15D}$ = 5.8 ± 0.24 pN and $F_{tension,\ top2\text{-}4\ 15D}$ = 5.4 ± 0.13 pN; $P = 0.12$, *t* test; Fig. 3 E). Thus, even though stiffness was reduced by approximately twofold in the *top2-4* mutant relative to WT, tension was similar in both cases (Fig. 3 E). In addition, analogous tension maintenance was observed in *bub1Δ* cells, which displayed a more moderate pericentromere stiffness phenotype (Fig. S2). Together, these results suggest that pericentromere tension is regulated by the spindle during mitosis to maintain a set point tension level (Maresca and Salmon, 2009).

Pericentromere tension is regulated by changes in spindle structure

Because our results suggested that the metaphase spindle acts to maintain a set point tension, we then explored possible mechanisms for how cells could maintain WT tension in the presence of altered pericentromere stiffness. By imaging cells with labeled spindle poles (SPC110-mCherry) and kinetochores (Nuf2-GFP; Fig. 4 A), we found that cells compensate for softer pericentromeres by altering spindle structure: spindle lengths were increased by 18% in *top2-4* cells as compared with WT cells (Fig. 4 B), and kMTs were 20% shorter (Fig. 4 C). Therefore, the net effect of a simultaneous increase in spindle length and a decrease in kMT length is that a set point WT tension is maintained even with a significant disruption in pericentromere stiffness (Fig. 4 D).

Because kMTs were shorter in the presence of softer *top2-4* chromatin, we then asked whether dynamic kMTs were required for tension regulation in yeast. This was performed by treating WT and *top2-4* spindles with low-dose benomyl, which has been previously reported to stabilize kMT dynamics (Fig. 4 E; Pearson et al., 2003). We found that tension regulation was not efficient in *top2-4* spindles treated with benomyl: the mean tension in benomyl-treated *top2-4* spindles was 27% lower than in benomyl-treated WT cells (Fig. 4 F, red arrows, $P < 0.0001$). In contrast, the mean tension was statistically indistinguishable between untreated WT and *top2-4* cells (Fig. 4 F, blue arrows, $P = 0.12$, *t* test). Importantly, the difference in spindle lengths between strains was similar in controls and in benomyl treatment (Fig. 4, B and G), meaning that the loss of tension regulation in benomyl-treated *top2-4* cells was specifically attributable to stabilization of kMT dynamics (Fig. 4, C, H, and I). We conclude that dynamic kMTs are required for tension regulation in yeast.

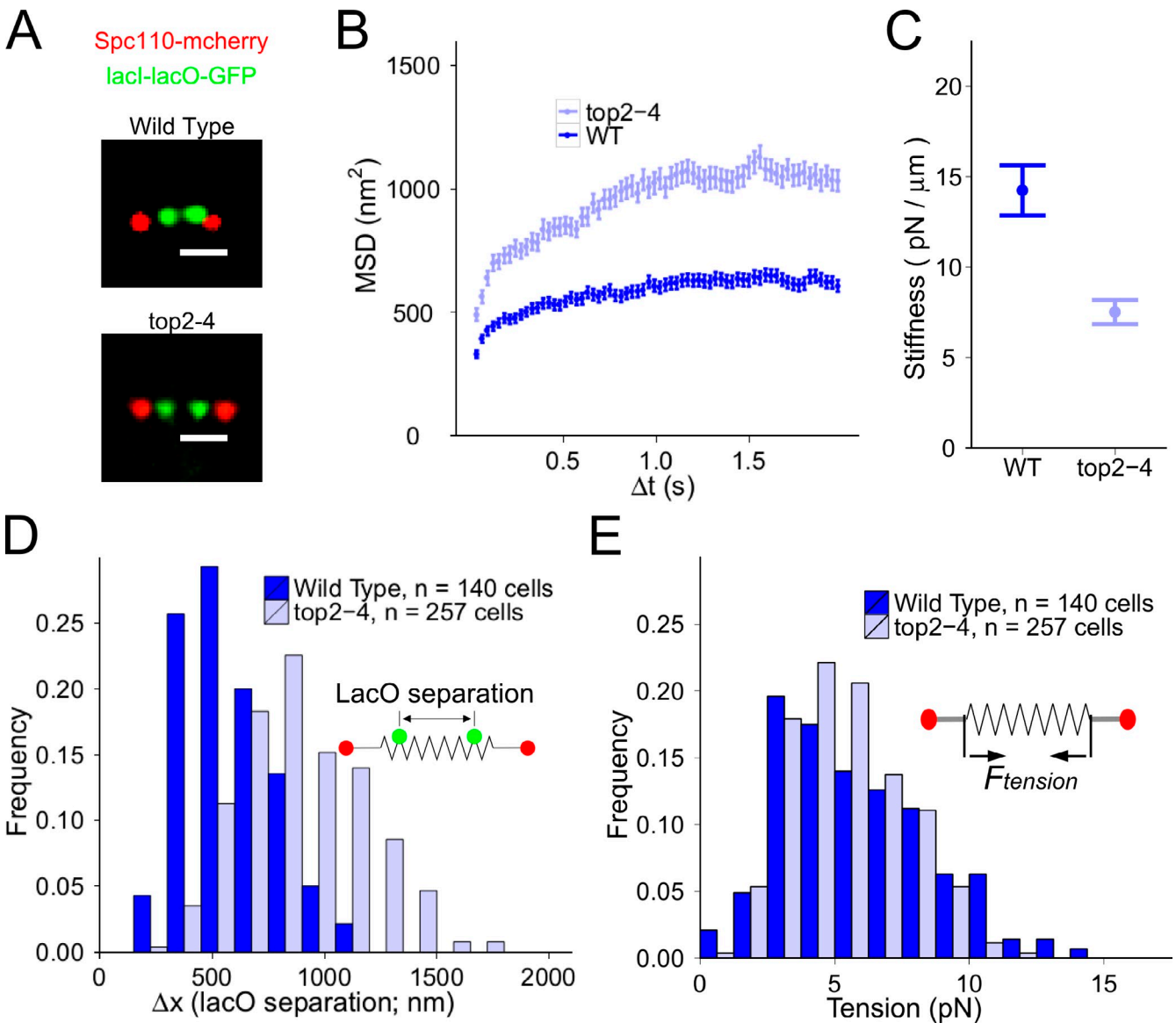

Figure 3. **Tension regulation in yeast metaphase spindles.** (A) WT and *top2-4* spindles, labeled as in Fig. 1. Bars, 1 μm. (B) MSD versus time step size in WT (light blue) and *top2-4* (dark blue) cells. (C) Pericentromere stiffness. (D) lacO spot separation distances in WT cells and in *top2-4* cells ($P < 0.0001$, *t* test). (E) Pericentromere tension distributions are similar between WT and *top2-4* cells ($P = 0.12$, *t* test). Error bars = SEMs.

Simulations predict that tension-dependent kMT dynamics can explain tension regulation

It has been previously proposed that kMT dynamics are regulated by tension (Gardner et al., 2005; Asbury et al., 2006; Ribeiro et al., 2009; Akiyoshi et al., 2010). Thus, a possible mechanism for tension regulation is that kMT dynamics are responsive to pericentromere stiffness changes, so that kMTs would maintain proper tension by self-adjusting their lengths. To test whether tension-dependent kMT dynamics can explain pericentromere tension regulation, we performed metaphase spindle simulations in which each kMT "sensed" tension (Gardner et al., 2005). Here, the probability of a kMT rescue event (i.e., a switch from shortening to growing) increased with increasing pericentromere tension, in which tension was calculated as $F_{tension} = \kappa_{sim}(\Delta x - \Delta x_{rest})$ (Δx = distance between simulated sister kinetochores, and κ_{sim} = pericentromere stiffness; Fig. 5 A).

Initially, WT simulations were run to obtain agreement between WT experimental and simulated images (see Materials and methods). The WT simulation value for pericentromere stiffness was thus established as $\kappa_{sim,WT} = \kappa_{exp,WT} = 14.2$ pN/μm (Fig. 5 B). Then, the simulations were used to test hypotheses for tension regulation in yeast. We first asked whether increasing the WT-simulated spindle lengths to match the experimentally observed *top2-4* spindle lengths (i.e., without changing κ_{sim}) would be sufficient to reproduce the experimental *top2-4* kinetochore distribution. However, these simulations did not recapitulate the *top2-4* experimental results (Fig. 5 C), suggesting that a passive whole-spindle force balance (leading to longer spindle lengths in *top2-4* mutants) is insufficient by itself to explain tension

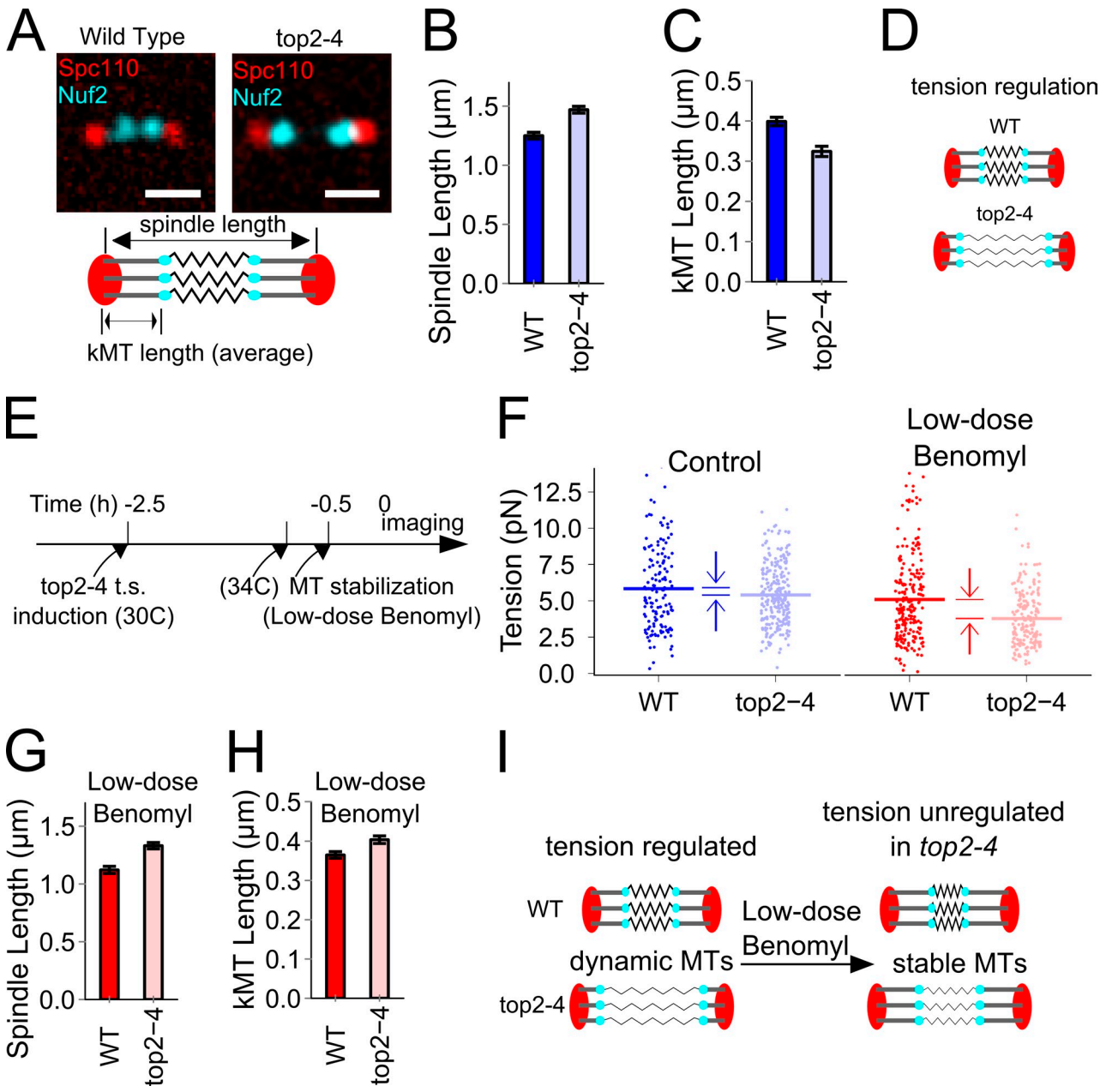

Figure 4. **Tension is regulated by spindle structure.** (A) Spindle and kMT lengths were measured in cells labeled with Spc110-mCherry and Nuf2-GFP. Bars, 1 µm. (B and C) Spindle length (B) and kMT length (C) in *top2-4* and WT cells. (D) Tension regulation in *top2-4* is accomplished via shorter kMT lengths and longer spindle lengths. (E) Experimental method to test whether dynamic kMTs are required to regulate tension in *top2-4* cells. (F) In untreated cells, WT tension is maintained regardless of pericentromere stiffness (blue), but in cells treated with low-dose benomyl, which stabilizes kMTs, tension is reduced in *top2-4* (red; control: $n = 140$ [WT] and $n = 257$ [*top2-4*]; benomyl: $n = 215$ [WT] and $n = 197$ [*top2-4*]). Horizontal lines and arrows are arithmetic means. (G) In benomyl, the relative difference in spindle length between WT and *top2-4* is similar to untreated cells (vs. B). (H) In contrast, kMTs after benomyl treatment are longer in *top2-4* (vs. C). (I) Tension regulation in *top2-4* is disrupted when kMTs are stabilized in benomyl. Error bars = SEMs.

regulation. In contrast, simulations in which the pericentromere stiffness was reduced to a value that was similar to the experimentally measured *top2-4* value ($\kappa_{sim,\ top2\text{-}4} = \sim 6.5$ pN/µm) produced a much better fit to the *top2-4* kinetochore distributions, both in simulations that used WT spindles lengths (Fig. 5 D) and in simulations with the *top2-4* spindle lengths (Fig. 5 E). Therefore, from the simulations, we conclude that tension-dependent kMT dynamics provide a simple, robust mechanism to explain how kMT lengths could self-adjust to changes in pericentromere stiffness and thus act to maintain a set point pericentromere tension during metaphase.

In addition to tension-dependent kMT dynamics, the balance of forces in the spindle between outward force-generating molecular motors and passive inwardly directed pericentromere stretch also likely contributes to tension regulation, primarily through changes in total spindle length. However, although it is clear that this type of passive response tension regulation mechanism (i.e., through a whole-spindle force balance) could respond

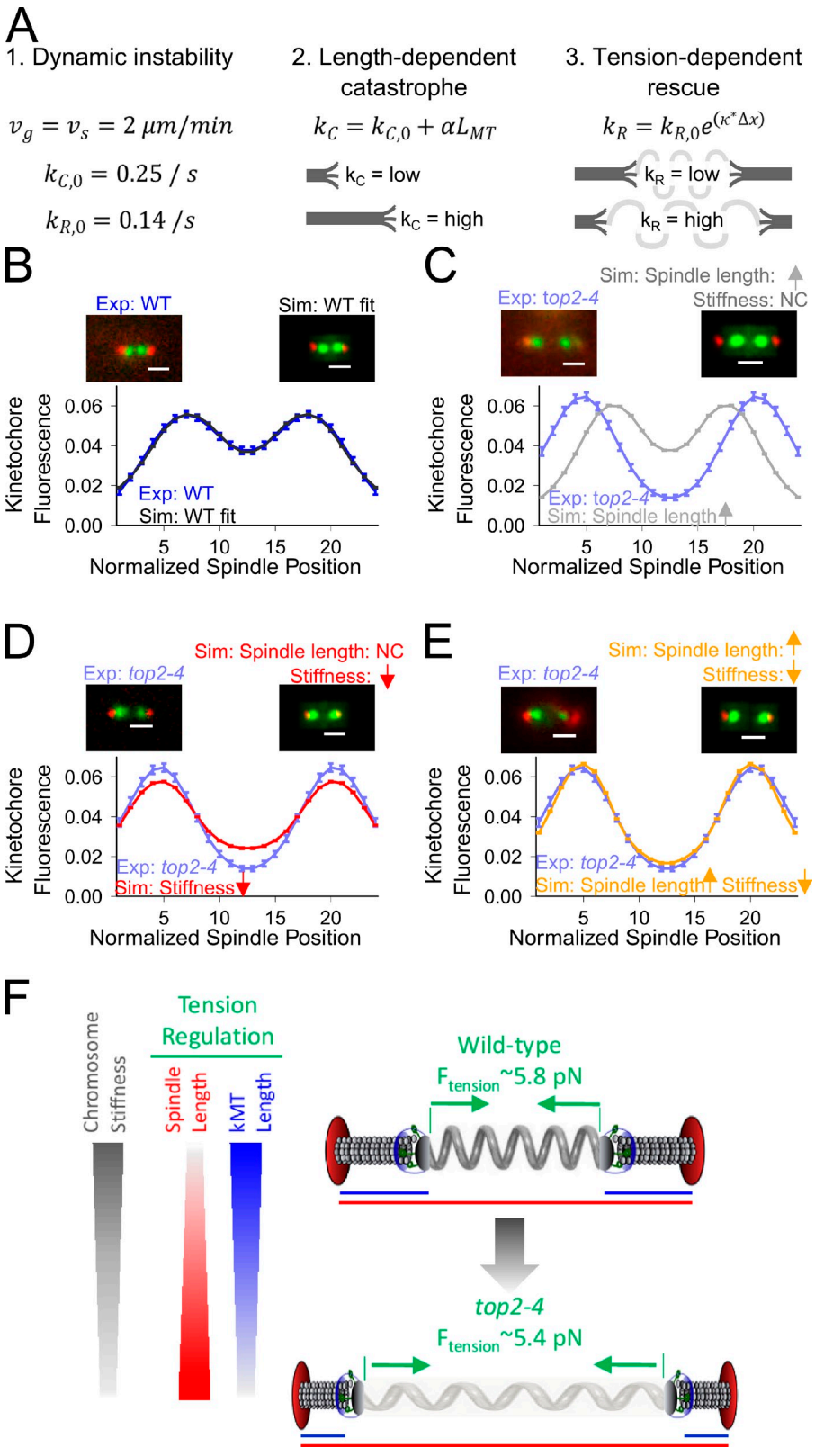

Figure 5. **In simulations, tension-dependent kMT dynamics can explain tension regulation.** (A) kMT dynamics in the simulation are governed by: (1) kMT dynamic instability with constant growth (v_g) and shortening (v_s) rates and with basal catastrophe ($k_{C,0}$) and rescue ($k_{R,0}$) frequencies; (2) kMT catastrophe frequency that increases with kMT length; and (3) kMT rescue frequency that increases with pericentromere tension. (B–E) Comparison of experimental images to simulated images convolved from the model (red, Spc110-mCherry; green, Nuf2-GFP). Bars, 1 µm. Exp = experimental image; Sim = simulated image; NC = no change. (B) WT experimental results compared with WT simulations. (C) *top2-4* experimental results compared with simulations using longer *top2-4* experimental spindle lengths with WT pericentromere stiffness. (D) *top2-4* experimental results compared with simulations using reduced pericentromere stiffness and WT experimental spindle lengths. (E) *top2-4* experimental results compared with simulations using reduced pericentromere stiffness and longer *top2-4* experimental spindle lengths. (F) Pericentromere tension is regulated by spindle structure: increased stretch of the softer *top2-4* pericentromere (light gray spring) relative to a stiffer WT pericentromere (dark gray) leads to similar tension ($F_{tension}$) because of increased spindle lengths and reduced kMT lengths. Error bars = SEMs.

to global changes in chromosome stiffness, it is less clear that this mechanism could compensate for stochastic variation in individual chromosome stiffness (Moser and Swedlow, 2011). In contrast, tension-dependent kMT dynamics could effectively regulate tension for each individual chromosome pair, to compensate for heterogeneity in stiffness across different chromosomes in the spindle or to compensate for stiffness changes in an individual chromosome over time (Chacón and Gardner, 2013; Stephens et al., 2013). It has long been suggested that mechanical tension at the kinetochore could modulate kMT

stability inside of cells (Nicklas, 1988; Skibbens et al., 1993, 1995; Rieder and Salmon, 1994, 1998; Inoué and Salmon, 1995; Skibbens and Salmon, 1997; Maddox et al., 2003; Cimini et al., 2004; Ribeiro et al., 2009). Thus, we propose that yeast kMTs sense tension, such that high forces promote net kMT polymerization, whereas low forces promote net depolymerization. As demonstrated by our simulations, this effect naturally leads to shorter kMTs in the presence of softer pericentromeres, as is experimentally observed for the yeast *top2-4* mutants, and thus provides a physically reasonable explanation for tension regulation in yeast metaphase.

Conclusions

In this work, we used a novel imaging-based method to measure pericentromere stiffness during metaphase and then applied our stiffness measurements to determine the magnitude of pericentromere tension in budding yeast. We found that the cell compensates for reductions in stiffness: the spindle length was increased, whereas the mean kMT length was decreased, to restore WT pericentromere tension in cells with reduced pericentromere stiffness (Fig. 5 F). This suggests that tension is regulated by the integrated dynamics of spindle length and kMT length during mitosis to achieve precise regulation of metaphase tension. This process could act to prevent transient reactivation of the spindle checkpoint during metaphase and thus ensure a timely anaphase onset.

Materials and methods

Yeast strains and imaging

Yeast strains are shown in Table S2. For imaging of the yeast cells, metaphase cells were imaged using a microscope (Eclipse Ti; Nikon) using 488- and 561-nm lasers. To optimize the signal to noise ratio in our assay, we used pseudo–total internal reflection fluorescence (TIRF; pseudo-TIRF) microscopy of cells that were adhered to coverslips in a flow chamber (i.e., TIRF microscopy but with the laser angle adjusted to increase evanescent field depth). A rapid switching FireWire setup allowed for near-simultaneous imaging between the red and green lasers. An electron-multiplying charge-coupled device camera (iXon$_3$; Andor Technology) fitted with a 2.5× projection lens was used to capture images with a 64-nm pixel size in the field of view. For time-lapse videos, cells were imaged at variable speeds using TIRF with a CFI Apochromat 100×, 1.49 NA oil objective (Nikon). The software NIS Elements (Nikon) was used for image acquisition.

Yeast cells were grown overnight at 26°C in 25 ml YPD (yeast peptone dextrose) + 100 µl of 100× adenine and then diluted into 15 ml SD + 100 µl of 100× adenine at 30°C (except as specified). To measure stiffness, cells were spun down and then resuspended in one of the following treatments for 20 min before imaging, SD, water, 0.02% azide in water, 0.02% azide and 1 mM deoxyglucose in water, or 0.02 mg/ml benomyl in water, and imaged at 26°C. The drug treatments were also used as the imaging buffer as applicable. These drugs were chosen as they have previously been shown to stabilize kMTs and motors (Marshall et al., 1997; Pearson et al., 2003). For the comparison of WT to *top2-4* strains, yeast cells (strain 15D; Fig. 3) were also grown in YPD + adenine and diluted into SD + adenine as in other treatments, except that *top2-4* is a temperature-sensitive mutant (Warsi et al., 2008). Therefore, dilutions were grown at 26°C and then shifted to the nonpermissive temperature (34°C) for 30 min before imaging. Imaging continued at the nonpermissive temperature. For benomyl treatments, which examined how the stabilization of kMT dynamics affected spindle length, kMT length, and tension, cells were spun and resuspended in 0.02 mg/ml benomyl in SD immediately before imaging, and imaging was stopped after 1 h.

Cells were immobilized on a coverslip to allow for TIRF imaging. To do this, we created flow chambers using a washed NaOH-treated coverslip, an untreated coverslip above the imaging coverslip to create a chamber, and thin strips of melted parafilm to separate the coverslips. We introduced concanavalin A into a flow chamber for 20 min at room temperature, which bound to the NaOH-treated coverslip. Excess concanavalin A was then washed out of the chamber and replaced with water. Cells were pipetted into the chamber and adhered to the concanavalin A–coated coverslip. Excess cells that did not adhere to the coverslip were removed with vacuum.

For stiffness calculations, final sample sizes using WT cells in strain background W303 were n = 27 cells over five experiments (H_2O at 32 fps), n = 17 cells over four experiments (SD at 32 fps), n = 9 cells over two experiments (SD at 48 fps), n = 11 cells over three experiments (azide in H_2O at 32 fps), n = 11 cells over three experiments (azide and deoxyglucose in H_2O at 32 fps), n = 26 cells over 11 experiments (azide in H_2O at 0.2 fps), and n = 13 cells over seven experiments (benomyl in H_2O at 0.2 fps). Sample sizes for the comparison of *top2-4* to WT in strain background 15D were n = 14 cells over two experiments (WT in H_2O at 32 fps) and n = 19 cells over two experiments (*top2-4* in H_2O at 32 fps). Sample size of *bub1Δ* cells was n = 15 cells over two experiments (SD at 32 fps).

Image analysis

Time-lapse videos were analyzed in MATLAB (MathWorks, Inc.) using a custom-written code (Supplemental material). This program did the following to each frame in order: First, an image was filtered using a fine-grain Gaussian filter (standard deviation = 1 pixel) to remove noise using fspecial. Next, a background image was created by applying fspecial with a coarser grain Gaussian filter (standard deviation = 30 pixels) to the image, and this background was subtracted from the noise-filtered image to produce the final image used for analysis. The locations of the spindle poles (Spc110-mCherry) and/or the chromatin tags (lacO/lacI-GFP) in yeast were determined using Gaussian mixture model fitting to find subpixel locations (Thomann et al., 2002; Jaqaman et al., 2008). Because there are two point sources in each case, a two-mixture iterative Gaussian fit was applied to a vector containing fluorescence intensity along the spindle axis integrated in a 15-pixel-wide band to obtain subpixel resolution locations of each spindle pole body or lacO spot, using the function gmdistribution.fit from the MATLAB statistics toolbox.

To compare mean kMT lengths in WT and *top2-4* yeast cells, we labeled strains so that the plus ends of kMTs were labeled at the outer kinetochore with the fusion protein Nuf2-GFP, and the minus ends of kMTs were labeled at the spindle pole body with the fusion protein Spc110-mCherry. The GFP fluorescence for each set of 16 kMTs on one side of the spindle midline appeared as one cluster (Fig. 4 A). We reasoned that the peak fluorescence location within each cluster would denote the mean plus-end location of the 16 kMTs per half-spindle. Therefore, mean kMT lengths within cells were determined from fluorescence distributions of outer kinetochore markers, as previously described (Gardner et al., 2005). In brief, we measured the GFP fluorescence from spindle pole to spindle pole, after determining the precise spindle pole locations using Gaussian mixture fitting to the pole fluorescence in 1D along the spindle axis. The peak fluorescence in each cell's half-spindle, our metric for mean location of the kMT plus end, was then determined as the point midway between the two pixels with the highest fluorescence intensity.

Sample sizes for kMT and spindle lengths were n = 78 cells over two experiments for WT control cells, n = 153 cells over two experiments for *top2-4* control cells, n = 94 cells over two experiments for WT cells treated with benomyl, and n = 125 cells over two experiments for *top2-4* cells treated with benomyl (Fig. 4, B, C, G, and H). Sample sizes for lacO separation and tension measurements were n = 140 cells over three experiments for control WT cells, n = 257 cells over three experiments for control *top2-4* cells, n = 215 cells over two experiments for WT cells treated with benomyl, and n = 197 cells over two experiments for *top2-4* cells treated with benomyl (Fig. 3, D and E; and Fig. 4 F). Sample size for lacO separation and tension measurements in *bub1Δ* was n = 154 cells over four experiments.

Evaluation of rest length for yeast metaphase pericentromeres

To estimate Δx_{rest} for yeast, we reduced $F_{tension}$ to 0 pN by treating cells with 15 µg/ml nocodazole, which depolymerizes kMTs and thus eliminates microtubule-associated pulling forces (Waters et al., 1996; Ribeiro et al., 2009). After treatment with 15 µg/ml nocodazole, the sister lacO spots collapse to one diffraction-limited spot, and so we calculated a maximum value of Δx_{rest} = 170 nm for yeast based on our light source and microscope objective (NA = lens NA): Rest length = diffraction limit = $\lambda/(2\ \mathrm{NA})$ = $\sim 500/(2 \times 1.49)$ = 170 nm.

This method provides a conservative upper bound for Δx_{rest} and is similar to our estimates using the superresolution bleaching-assisted localization microscopy method ($\Delta x_{rest,BALM}$ = ~140 nm [minimum value]; Burnette et al., 2011).

To measure $\Delta x_{rest,BALM}$, cells treated with nocodazole were continuously imaged (no delay) until complete bleach in the green (lacO) channel. Total magnification was 64 nm/pixel. We then used freely available ImageJ plugins (National Institutes of Health) to analyze the image stacks, as previously described (Burnette et al., 2011): (a) To correct drift in the images, we used the translational setting of StackReg, (b) bleaching/blinking off events and blinking on events were identified with the Delta F down setting and the Delta F up setting, respectively, of T-functions, and (c) bleaching-assisted localization microscopy molecules were localized, and image reconstructions were rendered by using QuickPALM. Single molecule localization was estimated by measuring dot locations in the final rendered images.

Pericentromere stiffness calculation method

To calculate yeast chromatin stiffness, we found the MSD of the lacO/lacI-GFP tags and then applied the equipartition theorem formula (Eq. 1), as follows (Fig. 1): (a) We collected time-lapse videos of metaphase yeast cells at the specified time interval while holding the stage at a constant temperature. (b) We found the distance between the lacO spots using our custom MATLAB script as described under Image analysis and then divided this distance by √2 to represent the motion of a single lacO spot. (c) We then calculated first differences and removed the effect of drift by fitting a line through a plot of the first differences over time for each cell. Residuals from this line were then used for the remainder of the analysis. In most cases, the slope of the line was not significantly different than 0, implying that little drift occurred. (d) To find the MSD for the cells within one treatment, we pooled the residuals from all cells. Next, we calculated the MSD using Eq. 2. We verified that pooling information across cells did not affect our results by randomly reordering the cells in the pool and then by verifying that results were consistent regardless of order.

For the fast imaging experiments, our MSD plots typically achieved a plateau by Δt = 0.5 s. Therefore, we estimated the MSD plateau value by averaging the MSD values from Δt = 1 s to Δt = 2 s. Some cells did not appear to plateau or had plateaus that were large outliers. These cells were identified by (a) finding the MSD plateau value from each individual cell, (b) making a histogram of the plateau MSD values from all cells, and then (c) fitting a two-mixture Gaussian model to this histogram for each treatment. In every case, the two-Gaussian mixture fit better than a single Gaussian, and there was usually a clean separation between the peaks. We discarded cells whose plateau was >2 standard deviations past the first peak, which when compared with the individual cell MSD plots, was indicative of an unstable maximum or a failure of the drug treatments.

The stiffness of an elastic polymer dictates the maximum amount a probe bound to the polymer is able to move at a particular temperature. The maximum MSD ($<\sigma^2>$) is the plateau in our MSD plots minus the intercept. Intuitively, an object cannot move in zero time, so any nonzero motion estimate at the intercept is erroneous (Michalet, 2010). In this study, we used the first MSD point as an estimate for the intercept, which is a combination of noise in the images, imperfect Gaussian fitting, and movement of the GFP tags during the time the shutter is open. This noise correction explains why some plateaus may appear similar (Fig. S2 B) and yet have different stiffness estimates (i.e., the *bub1Δ* intercept is lower and its plateau is higher than WT; Fig. S2 B). Finally, by knowing the temperature of the assay (T) and the net MSD ($<\sigma^2>$), we calculated the stiffness of the pericentromere along the spindle axis using Eq. 1.

To determine the standard error of the stiffness estimate, we propagated the error from the MSD data in three steps. First, because the estimate of the MSD plateau represented a mean of multiple MSD values from different cells, we found a mean error of these MSD values. This was performed by squaring each MSD's standard deviation, summing these values, dividing the summed value by the number of measurements, and then taking the square root. Next, because the measurement error in the stiffness estimate was composed of error in the plateau and the error in the noise estimate (first time point MSD), we propagated this error by taking the square root of the sum of the squared errors in the plateau value and the first time point (intercept). This value represented the error in $<\sigma^2>$. Finally, because the stiffness (κ) is a transformed value of $<\sigma^2>$, we propagated error by taking the derivative of the transformation function (Eq. 1), evaluating this derivative with the untransformed mean ($<\sigma^2>$), and then multiplying the result by the untransformed error in $<\sigma^2>$.

Justification of the in vivo stiffness measurement method

Capturing thermal fluctuations. As is expected with any new technique, there are several issues to be considered in regards to using an imaging-based method to measure pericentromere stiffness during mitosis. First, we note that our stiffness measurements are likely conservative because of the possibility that residual lacO spot motions derived from kMT and motor-driven forces could contribute to our measured MSD values, even with rapid image acquisition. However, our stiffness measurements using the rapid imaging method were statistically indistinguishable between live cells and in drugs that stabilized kMT dynamics and motor-driven forces. This suggests that (a) thermal fluctuations are dominating the analysis, and (b) the drug treatments did not substantially increase chromatin stiffness. In addition, the pericentromere stiffness measurements reported here are on the order of previously reported chromosome stiffness values that were measured with micromanipulation techniques (Nicklas, 1988; Kawamura et al., 2010; Gay et al., 2012). Finally, stiffness estimates from experiments with slow time-lapse imaging (0.2 fps) and without drugs to stabilize kMT/motor dynamics were substantially softer than in fast time-lapse and/or drug experiments (Fig. S1, D and E), suggesting that thermal fluctuations were dominating the fast time-lapse and/or drug stabilization experiments.

There are several lines of published evidence that support the assumption that the rapid time-lapse videos at 32 fps (or faster) captured lacO spot motion caused by thermal fluctuations: (a) In vivo astral microtubule dynamics in budding yeast have been directly measured and published. Specifically, both the growth and the shortening rates of budding yeast astral microtubules were measured in all stages of the cell cycle by various groups (see Gupta et al., 2006; Table S2). Here, regardless of stage, the overall microtubule growth rate in budding yeast was ∼1 µm/min, with a shortening rate of ∼2 µm/min. (b) The FRAP recovery time for GFP-Tub1 has been measured in budding yeast metaphase spindles to evaluate kMT turnover. Here, the total recovery time for a metaphase half-spindle was observed to be ∼250 s (Maddox et al., 2000; Pearson et al., 2006). Given the small size of the yeast mitotic spindle, kMTs residing in a half-spindle are typically ∼400 nm long, which suggests that mean kMT growth and shortening rates are slow. (c) Our previous modeling efforts recapitulated proper spatial FRAP recovery times in the budding yeast metaphase spindle with growth and shortening rates of 1.2 µm/min (Pearson et al., 2006).

Therefore, consistent with published literature, we expect that microtubule growth and shortening rates in budding yeast are ∼2 µm/min, which would contribute ∼1 nm of movement in each time step at 32 fps. This is well below the estimated measurement noise of our assay (MSD for first time step is typically ∼300 nm^2, leading to a noise estimate of √300 = 17 nm). In support of this conclusion, imaging at 48 fps did not result in stiffer pericentromere estimates (Fig. 2), and drug treatments that stabilize kMT and or motor dynamics did not significantly increase stiffness (Fig. 2). Finally, stiffness estimates that were made without fast imaging or drug treatments were an order of magnitude softer than in our fast time-lapse or drug-treated stiffness experiments, suggesting that the substantial majority of active forces were stabilized over the time scale of our experiments (Fig. S1, D and E).

Imaging intact spindles. We were careful to perform our analysis using intact metaphase spindles with pericentromeric tags. Therefore, our results elucidate pericentromere tension at a spindle location and stage of mitosis in which tension is thought to provide an important mechanochemical signal. One concern may be that because intact spindles were used for the analysis, it is possible that flexible connections between kinetochores and microtubules, as well as between microtubules and spindle poles, could contribute to the measured MSD values. However, we reason that these connections are likely to be much stiffer than the relatively flexible chromosomes and will therefore not contribute substantially to our measurements. This assumption is supported by our results, which demonstrate that the stiffness measurement assay is sensitive to a mutation that affects chromosome-associated topoisomerase II (Fig. 3 C) because if the stiffness measurements were dominated by the flexibility of spindle components other than chromosomes, these stiffness changes would not have been detected.

Another potential concern in using intact spindles is that the proximity of the kinetochores to the lacO spots could constrain movements of the lacO spots toward the kinetochore (i.e., the lacO spots would "bump" into the kinetochore), artificially inflating our stiffness estimates. Here, there would be a higher stiffness estimate near to the kinetochore barrier, whereas the stiffness away from the kinetochore would be represented by the movement of tags that are unconstrained by bumping into a barrier (Verdaasdonk et al., 2013). However, for our metaphase measurements, because we stabilized the motor and microtubule dynamics over the time course of the experiments, the total observed displacements were very small. Therefore, it is unlikely that our metaphase lacO displacements were large enough to bump into the tether point at the kinetochore. Regardless, because we observed 1D lacO distances along the spindle axis, we expect that if the lacO spot movements were indeed restricted in one direction by the proximity of the lacO marker to the kinetochore, a statistically significant skew would be present in the lacO displacement data. This is because displacements toward larger lacO spacings would be limited by the presence of the kinetochore,

and so the distribution would be cut off at larger displacements, skewing the distribution of lacO displacements toward smaller lacO spacings. We tested this by calculating the skew in our largest dataset, the W303 WT cells imaged in H_2O (Fig. S1 C), and found that the data do not significantly deviate from a normal distribution when assessed using a D'Agostino skewness test (residuals: P = 0.22; raw lacO spacing data: P = 0.88). We conclude that by eliminating the effects of motor and microtubule dynamics via drugs and fast imaging, and also by ensuring that the motions of the lacO spot were not restricted by the proximity of the kinetochore-attached microtubule tip, we have eliminated potential position-dependent artifacts of the stiffness measurement in our study.

Spindle axis positioning of lacO spots. The lacO spots were generally well in line with the mCherry-labeled spindle poles, and no consistent spindle offset was observed. Regardless, because we measured the fluctuations in lacO spacing along the spindle axis, we expect that stiffness along the spindle axis would still be reflected even if the lacO spots were contained in an off-axis chromatin loop. Specifically, if the lacO spots were off axis, their along-axis spacing fluctuations would still reflect along-axis thermal fluctuations of the pericentromere because the tag would travel along with fluctuations in the pericentromere itself. Therefore, regardless of whether the tags were directly in line with the spindle axis or slightly offset, as long as they are associated with the pericentromere, their motion as a result of thermal forces will be dictated by the mean stiffness of the pericentromere.

Estimating single spot motion from the distance between both lacO spots. Division of the lacO spot separation distance by $\sqrt{2}$ to estimate single spot motion was justified as follows: (a) by generating simulated data of two independently moving lacO spots, we demonstrated that halving the MSD of the distance between two spots (i.e., dividing the Δx_i displacement by $\sqrt{2}$) was equivalent to estimating the MSD of each single spot (Fig. S1 A), and (b) by calculating cross-correlation between individual lacO spot positions, we demonstrated that the experimental sister lacO spot movements were independent and uncorrelated (Fig. S1 B), as is required for estimation of single spot MSDs from the Δx_i displacements.

To demonstrate that the MSD of each individual lacO spot can be estimated by dividing lacO spacing displacements (Δx_i) by $\sqrt{2}$, we simulated 10^4 time steps of constrained diffusion of two independent spots, which were centered at different locations but had the same diffusion coefficients and level of constraint. We then calculated $\Delta x_i/\sqrt{2}$. Plots of these are shown in Fig. S1 A (left). The MSD curve of $\Delta x_i/\sqrt{2}$ is similar to the individual spot curves, which demonstrates that the distance between the spots can be used to estimate the mean single spot motion (Fig. S1 A, right).

To demonstrate that the experimental sister lacO spot movements were independent and uncorrelated, we calculated cross-correlation of lacO spot locations in the same cell and across cells (Fig. S1 B). The lacO spot motions are similarly uncorrelated in each case, demonstrating that sister lacO spot motions are uncorrelated.

Linearity of pericentromere stiffness

We also asked whether our measured pericentromere stiffness values depended on the separation distance, or amount of pericentromere stretch, between sister lacO spots. To perform this analysis, we noted that the lacO spot separation distances used for the MSD analysis varied from 400 to 800 nm (Fig. S2 F). We compared the stiffness of three groups that were distinguished by increasing lacO spot separation distances using the MSD analysis (Fig. S2 G) and found no statistically significant change in stiffness between the groups of cells with the smallest and largest lacO spot separation distances (P = 0.11 for fast time-lapse data of untreated cells imaged in water; Fig. S2 H). Consistent with this result, the force-extension curves of chromosomes pulled with needles were also linear over biologically relevant forces (Nicklas and Koch, 1969; Kawamura et al., 2010). However, because there is a trend in the direction of lower stiffness at higher amounts of stretch, we also calculated tension forces using the specific stiffness values for each lacO spot separation distance (Fig. S2 I). The mean tension was not significantly altered by this approach (4.5 vs. 4.6 pN), and therefore, we conclude that the use of a mean stiffness is a reasonable approximation for our study.

Statistical analyses

To compare stiffness between treatments, we conducted two-sided *t* tests using Welch's *t* test assuming unequal sample size and unequal variance. Variance and degrees of freedom were determined as described under Pericentromere stiffness calculation method. We only conducted one *t* test to determine whether WT yeast stiffness changed as a function of chromatin stretch (Fig. 1 F); because the greatest difference was not significant, we did not conduct further tests and therefore did not need to correct for multiple comparisons. Two-sided *t* tests using Welch's *t* test assuming unequal sample size and unequal variance were also used to compare tension, spindle length, and kMT length between treatments. To examine how the effect of benomyl treatment on tension or kMT length may be different depending on genotype, we conducted a two-way analysis of variance. To determine whether there was significant skew in histograms of residual values, we used the D'Agostino test implemented in the moments package in R. Analyses were conducted in R.

Estimation of thermal forces in metaphase spindles

To calculate the thermal tension value for yeast spindles, we assumed that the total energy available to an individual pericentromere during mitosis was equal to 1 k_BT. This amount of energy is equal to ~4 pN–nm. Therefore, taking into account a mean stretch distance in yeast of $\Delta x_{mean} - \Delta x_{rest}$ of 499 − 170 = 329 nm, the expected $F_{tension}$ as a result of thermal energy alone would be $F_{tension,\ thermal}$ = 4/329 = ~0.01 pN.

Simulation methods

The computational simulation used for mitotic kMT dynamics was based in large part on that described in Gardner et al. (2005). The model was composed of 16 oppositely oriented pairs of dynamic kMTs within a preset spindle length (x axis), and whose minus-end z–y positions were randomly chosen within a circle of radius of 125 nm, to simulate spindle poles. The kMTs' behavior was dictated by three rules. First, individual kMTs were governed by dynamic instability parameters, such that kMT growth and shortening occurred at a rate of 2 µm/min, and the basal catastrophe frequency (switch from growth to shortening) and rescue frequency (switch from shortening to growth) were 0.25 and 0.14 s^{-1}, respectively. The second rule affected how the catastrophe frequency changed with the length of the kMT. In the previous model, catastrophe frequency increased with a nonlinear gradient toward the spindle midzone (Gardner et al., 2005), but more recent work suggests that catastrophe frequency increases linearly with kMT length (Gardner et al., 2008). Therefore, the catastrophe frequency of a specific growing kMT was determined by $k_c = k_{c,0} + \alpha L_{MT}$, in which k_C was the catastrophe frequency ($seconds^{-1}$), $k_{C,0}$ was the basal catastrophe frequency ($seconds^{-1}$), L_{MT} was the kMT's length (micrometers), and α was a free parameter with units of $micrometers^{-1}$ $seconds^{-1}$, which established how relating how kMT length affected catastrophe.

The final rule in the model dictated how tension caused by stretching of elastic chromatin between paired kMTs affected the kMTs' chance of rescue from a shortening state. Gardner et al. (2005) assumed that tension modifies the baseline chance of rescue by

$$k_R = k_{R,0} e^{(\kappa^* \Delta x)},$$

in which k_R was the rescue frequency ($seconds^{-1}$), $k_{R,0}$ was the basal rescue frequency ($seconds^{-1}$), and Δx was the amount by which the chromatin was stretched (micrometers). $\kappa^* = \kappa/F_0$, which incorporates both the experimentally measured stiffness of the pericentromere κ (piconewton/micrometers) as well as F_0 (piconewtons), which is the characteristic force at which the chance of rescue increases e-fold.

To constrain the free parameters in the model that are not of direct interest (α and F_0), we created simulated spindle images from our models and compared these directly to experimental data. First, we simulated spindles with spindle lengths equal to those measured in vivo using WT cells (same WT data as in Fig. 4, B and C). At the end of the simulation, the positions of the plus ends of kMTs, as well as the positions of the spindle poles, were convolved using the point-spread function of our microscope, and simulated images were generated from these convolutions (Sprague et al., 2003; Gardner et al., 2010). Simulated fluorescence intensity along the spindle axis was calculated for such models over many values of α and F_0. We directly compared these simulated fluorescence curves to data from live cells whose kMT plus ends were labeled with GFP (Nuf2-GFP) and whose spindle poles were labeled with mCherry (Spc110-mCherry). Once we obtained a good fit to WT images, which occurred at $\kappa^* = 2.75$ μm^{-1} and $\alpha = 120$ μm^{-1} s^{-1}, we fixed κ to our experimental value (κ_{WT} =14.2 pN/µm) and therefore held F_0 and α as constants ($F_0 = 5.15$; $\alpha = 120$) in subsequent simulations.

Once we found parameter values that led to a reasonable fit between the model and the experimental WT data, we tested the hypothesis that in *top2-4* cells, softer pericentromeres led to the shortened kMTs that were experimentally observed in vivo. We did this by simulating spindles

whose spindle lengths matched those observed in *top2-4* cells or in WT cells and by varying κ, creating simulated images, and finding the best match to the experimental data.

Online supplemental material

Fig. S1 provides additional data to justify assumptions inherent in the chromatin stiffness calculations and a linear spring analysis. Fig. S2 includes an experiment, which demonstrated that tension self-regulation occured in a *bub1Δ* mutant strain. Table S1 provides a summary of in vivo mitotic force measurements. Table S2 provides a list of strains used in this study. Video 1 is an animated cartoon, which demonstrates how thermal fluctuations of lacO spots can be used to estimate metaphase chromatin stiffness (equipartition theorem). A ZIP file is also provided containing the MATLAB script used to measure distance between lacO spots for stiffness measurements. Online supplemental material is available at http://www.jcb.org/cgi/content/full/jcb.201312024/DC1.

We thank Dr. Trisha Davis for the generous gift of strains and Dr. David Odde for helpful suggestions.

Funding was provided by the Pew Scholars Program in the Biomedical Sciences and by the National Institutes of Health National Institute of General Medical Sciences grant GM-100122 to M.K. Gardner. J.M. Chacón was supported in part by Postdoctoral Fellowship no. 124521-PF-13-109-01-CCG from the American Cancer Society.

The authors declare no competing financial interests.

Submitted: 4 December 2013
Accepted: 8 April 2014

References

Akiyoshi, B., K.K. Sarangapani, A.F. Powers, C.R. Nelson, S.L. Reichow, H. Arellano-Santoyo, T. Gonen, J.A. Ranish, C.L. Asbury, and S. Biggins. 2010. Tension directly stabilizes reconstituted kinetochore-microtubule attachments. *Nature*. 468:576–579. http://dx.doi.org/10.1038/nature09594

Alexander, S.P., and C.L. Rieder. 1991. Chromosome motion during attachment to the vertebrate spindle: initial saltatory-like behavior of chromosomes and quantitative analysis of force production by nascent kinetochore fibers. *J. Cell Biol.* 113:805–815. http://dx.doi.org/10.1083/jcb.113.4.805

Asbury, C.L., D.R. Gestaut, A.F. Powers, A.D. Franck, and T.N. Davis. 2006. The Dam1 kinetochore complex harnesses microtubule dynamics to produce force and movement. *Proc. Natl. Acad. Sci. USA*. 103:9873–9878. http://dx.doi.org/10.1073/pnas.0602249103

Bakhoum, S.F., S.L. Thompson, A.L. Manning, and D.A. Compton. 2009. Genome stability is ensured by temporal control of kinetochore-microtubule dynamics. *Nat. Cell Biol.* 11:27–35. http://dx.doi.org/10.1038/ncb1809

Bouck, D.C., and K. Bloom. 2007. Pericentric chromatin is an elastic component of the mitotic spindle. *Curr. Biol.* 17:741–748. http://dx.doi.org/10.1016/j.cub.2007.03.033

Burnette, D.T., P. Sengupta, Y. Dai, J. Lippincott-Schwartz, and B. Kachar. 2011. Bleaching/blinking assisted localization microscopy for superresolution imaging using standard fluorescent molecules. *Proc. Natl. Acad. Sci. USA*. 108:21081–21086. http://dx.doi.org/10.1073/pnas.1117430109

Bustamante, C., J.C. Macosko, and G.J. Wuite. 2000. Grabbing the cat by the tail: manipulating molecules one by one. *Nat. Rev. Mol. Cell Biol.* 1:130–136. http://dx.doi.org/10.1038/35040072

Chacón, J.M., and M.K. Gardner. 2013. Analysis and modeling of chromosome congression during mitosis in the chemotherapy drug cisplatin. *Cell. Mol. Bioeng*. 6:406–417. http://dx.doi.org/10.1007/s12195-013-0306-7

Cimini, D., L.A. Cameron, and E.D. Salmon. 2004. Anaphase spindle mechanics prevent mis-segregation of merotelically oriented chromosomes. *Curr. Biol.* 14:2149–2155. http://dx.doi.org/10.1016/j.cub.2004.11.029

DiNardo, S., K. Voelkel, and R. Sternglanz. 1984. DNA topoisomerase II mutant of *Saccharomyces cerevisiae*: topoisomerase II is required for segregation of daughter molecules at the termination of DNA replication. *Proc. Natl. Acad. Sci. USA*. 81:2616–2620. http://dx.doi.org/10.1073/pnas.81.9.2616

Dumont, S., and T.J. Mitchison. 2009. Force and length in the mitotic spindle. *Curr. Biol.* 19:R749–R761. http://dx.doi.org/10.1016/j.cub.2009.07.028

Gardner, M.K., C.G. Pearson, B.L. Sprague, T.R. Zarzar, K. Bloom, E.D. Salmon, and D.J. Odde. 2005. Tension-dependent regulation of microtubule dynamics at kinetochores can explain metaphase congression in yeast. *Mol. Biol. Cell*. 16:3764–3775. http://dx.doi.org/10.1091/mbc.E05-04-0275

Gardner, M.K., D.C. Bouck, L.V. Paliulis, J.B. Meehl, E.T. O'Toole, J. Haase, A. Soubry, A.P. Joglekar, M. Winey, E.D. Salmon, et al. 2008. Chromosome congression by Kinesin-5 motor-mediated disassembly of longer kinetochore microtubules. *Cell*. 135:894–906. http://dx.doi.org/10.1016/j.cell.2008.09.046

Gardner, M.K., B.L. Sprague, C.G. Pearson, B.D. Cosgrove, A.D. Bicek, K. Bloom, E.D. Salmon, and D.J. Odde. 2010. Model convolution: A computational approach to digital image interpretation. *Cell. Mol. Bioeng*. 3:163–170. http://dx.doi.org/10.1007/s12195-010-0101-7

Gay, G., T. Courtheoux, C. Reyes, S. Tournier, and Y. Gachet. 2012. A stochastic model of kinetochore–microtubule attachment accurately describes fission yeast chromosome segregation. *J. Cell Biol.* 196:757–774. http://dx.doi.org/10.1083/jcb.201107124

Grishchuk, E.L., M.I. Molodtsov, F.I. Ataullakhanov, and J.R. McIntosh. 2005. Force production by disassembling microtubules. *Nature*. 438:384–388. http://dx.doi.org/10.1038/nature04132

Gupta, M.L., Jr., P. Carvalho, D.M. Roof, and D. Pellman. 2006. Plus end-specific depolymerase activity of Kip3, a kinesin-8 protein, explains its role in positioning the yeast mitotic spindle. *Nat. Cell Biol.* 8:913–923. http://dx.doi.org/10.1038/ncb1457

Haase, J., A. Stephens, J. Verdaasdonk, E. Yeh, and K. Bloom. 2012. Bub1 kinase and Sgo1 modulate pericentric chromatin in response to altered microtubule dynamics. *Curr. Biol.* 22:471–481. http://dx.doi.org/10.1016/j.cub.2012.02.006

Howard, J. 2001. Mechanics of Motor Proteins and the Cytoskeleton. Sinauer Associates, Sundeland, MA. 367 pp.

Inoué, S., and E.D. Salmon. 1995. Force generation by microtubule assembly/disassembly in mitosis and related movements. *Mol. Biol. Cell*. 6:1619–1640. http://dx.doi.org/10.1091/mbc.6.12.1619

Jaqaman, K., D. Loerke, M. Mettlen, H. Kuwata, S. Grinstein, S.L. Schmid, and G. Danuser. 2008. Robust single-particle tracking in live-cell time-lapse sequences. *Nat. Methods*. 5:695–702. http://dx.doi.org/10.1038/nmeth.1237

Kamiti, M., and T.G.M. van De Ven. 1996. Measurement of spring constants of polyacrylamide chains bridging particles to a solid surface. *Macromolecules*. 29:1191–1194. http://dx.doi.org/10.1021/ma950173m

Kawamura, R., L.H. Pope, M.O. Christensen, M. Sun, K. Terekhova, F. Boege, C. Mielke, A.H. Andersen, and J.F. Marko. 2010. Mitotic chromosomes are constrained by topoisomerase II–sensitive DNA entanglements. *J. Cell Biol.* 188:653–663. http://dx.doi.org/10.1083/jcb.200910085

Khodjakov, A., and J. Pines. 2010. Centromere tension: a divisive issue. *Nat. Cell Biol.* 12:919–923. http://dx.doi.org/10.1038/ncb1010-919

Levi, V., Q. Ruan, M. Plutz, A.S. Belmont, and E. Gratton. 2005. Chromatin dynamics in interphase cells revealed by tracking in a two-photon excitation microscope. *Biophys. J.* 89:4275–4285. http://dx.doi.org/10.1529/biophysj.105.066670

Maddox, P.S., K.S. Bloom, and E.D. Salmon. 2000. The polarity and dynamics of microtubule assembly in the budding yeast *Saccharomyces cerevisiae*. *Nat. Cell Biol.* 2:36–41. http://dx.doi.org/10.1038/71357

Maddox, P., A. Straight, P. Coughlin, T.J. Mitchison, and E.D. Salmon. 2003. Direct observation of microtubule dynamics at kinetochores in *Xenopus* extract spindles: implications for spindle mechanics. *J. Cell Biol.* 162:377–382. http://dx.doi.org/10.1083/jcb.200301088

Maresca, T.J., and E.D. Salmon. 2009. Intrakinetochore stretch is associated with changes in kinetochore phosphorylation and spindle assembly checkpoint activity. *J. Cell Biol.* 184:373–381. http://dx.doi.org/10.1083/jcb.200808130

Marshall, W.F., A. Straight, J.F. Marko, J. Swedlow, A. Dernburg, A. Belmont, A.W. Murray, D.A. Agard, and J.W. Sedat. 1997. Interphase chromosomes undergo constrained diffusional motion in living cells. *Curr. Biol.* 7:930–939. http://dx.doi.org/10.1016/S0960-9822(06)00412-X

Marshall, W.F., J.F. Marko, D.A. Agard, and J.W. Sedat. 2001. Chromosome elasticity and mitotic polar ejection force measured in living *Drosophila* embryos by four-dimensional microscopy-based motion analysis. *Curr. Biol.* 11:569–578. http://dx.doi.org/10.1016/S0960-9822(01)00180-4

Michalet, X. 2010. Mean square displacement analysis of single-particle trajectories with localization error: Brownian motion in an isotropic medium. *Phys. Rev. E Stat. Nonlin. Soft Matter Phys.* 82:041914. http://dx.doi.org/10.1103/PhysRevE.82.041914

Mickey, B., and J. Howard. 1995. Rigidity of microtubules is increased by stabilizing agents. *J. Cell Biol.* 130:909–917. http://dx.doi.org/10.1083/jcb.130.4.909

Moser, S.C., and J.R. Swedlow. 2011. How to be a mitotic chromosome. *Chromosome Res.* 19:307–319. http://dx.doi.org/10.1007/s10577-011-9198-3

Nicklas, R.B. 1988. The forces that move chromosomes in mitosis. *Annu. Rev. Biophys. Biophys. Chem.* 17:431–449. http://dx.doi.org/10.1146/annurev.bb.17.060188.002243

Nicklas, R.B., and C.A. Koch. 1969. Chromosome micromanipulation. 3. Spindle fiber tension and the reorientation of mal-oriented chromosomes. *J. Cell Biol.* 43:40–50. http://dx.doi.org/10.1083/jcb.43.1.40

Pearson, C.G., P.S. Maddox, E.D. Salmon, and K. Bloom. 2001. Budding yeast chromosome structure and dynamics during mitosis. *J. Cell Biol.* 152:1255–1266. http://dx.doi.org/10.1083/jcb.152.6.1255

Pearson, C.G., P.S. Maddox, T.R. Zarzar, E.D. Salmon, and K. Bloom. 2003. Yeast kinetochores do not stabilize Stu2p-dependent spindle microtubule dynamics. *Mol. Biol. Cell*. 14:4181–4195. http://dx.doi.org/10.1091/mbc.E03-03-0180

Pearson, C.G., M.K. Gardner, L.V. Paliulis, E.D. Salmon, D.J. Odde, and K. Bloom. 2006. Measuring nanometer scale gradients in spindle microtubule dynamics using model convolution microscopy. *Mol. Biol. Cell*. 17:4069–4079. http://dx.doi.org/10.1091/mbc.E06-04-0312

Poirier, M.G., S. Eroglu, and J.F. Marko. 2002. The bending rigidity of mitotic chromosomes. *Mol. Biol. Cell*. 13:2170–2179.

Ribeiro, S.A., J.C. Gatlin, Y. Dong, A. Joglekar, L. Cameron, D.F. Hudson, C.J. Farr, B.F. McEwen, E.D. Salmon, W.C. Earnshaw, and P. Vagnarelli. 2009. Condensin regulates the stiffness of vertebrate centromeres. *Mol. Biol. Cell*. 20:2371–2380. http://dx.doi.org/10.1091/mbc.E08-11-1127

Rieder, C.L., and E.D. Salmon. 1994. Motile kinetochores and polar ejection forces dictate chromosome position on the vertebrate mitotic spindle. *J. Cell Biol.* 124:223–233. http://dx.doi.org/10.1083/jcb.124.3.223

Rieder, C.L., and E.D. Salmon. 1998. The vertebrate cell kinetochore and its roles during mitosis. *Trends Cell Biol*. 8:310–318. http://dx.doi.org/10.1016/S0962-8924(98)01299-9

Skibbens, R.V., and E.D. Salmon. 1997. Micromanipulation of chromosomes in mitotic vertebrate tissue cells: tension controls the state of kinetochore movement. *Exp. Cell Res.* 235:314–324. http://dx.doi.org/10.1006/excr.1997.3691

Skibbens, R.V., V.P. Skeen, and E.D. Salmon. 1993. Directional instability of kinetochore motility during chromosome congression and segregation in mitotic newt lung cells: a push-pull mechanism. *J. Cell Biol.* 122:859–875. http://dx.doi.org/10.1083/jcb.122.4.859

Skibbens, R.V., C.L. Rieder, and E.D. Salmon. 1995. Kinetochore motility after severing between sister centromeres using laser microsurgery: evidence that kinetochore directional instability and position is regulated by tension. *J. Cell Sci.* 108:2537–2548.

Sprague, B.L., C.G. Pearson, P.S. Maddox, K.S. Bloom, E.D. Salmon, and D.J. Odde. 2003. Mechanisms of microtubule-based kinetochore positioning in the yeast metaphase spindle. *Biophys. J.* 84:3529–3546. http://dx.doi.org/10.1016/S0006-3495(03)75087-5

Stephens, A.D., R.A. Haggerty, P.A. Vasquez, L. Vicci, C.E. Snider, F. Shi, C. Quammen, C. Mullins, J. Haase, R.M. Taylor II, et al. 2013. Pericentric chromatin loops function as a nonlinear spring in mitotic force balance. *J. Cell Biol.* 200:757–772. http://dx.doi.org/10.1083/jcb.201208163

Svoboda, K., C.F. Schmidt, B.J. Schnapp, and S.M. Block. 1993. Direct observation of kinesin stepping by optical trapping interferometry. *Nature*. 365:721–727. http://dx.doi.org/10.1038/365721a0

Thomann, D., D.R. Rines, P.K. Sorger, and G. Danuser. 2002. Automatic fluorescent tag detection in 3D with super-resolution: application to the analysis of chromosome movement. *J. Microsc.* 208:49–64. http://dx.doi.org/10.1046/j.1365-2818.2002.01066.x

Thompson, S.L., S.F. Bakhoum, and D.A. Compton. 2010. Mechanisms of chromosomal instability. *Curr. Biol.* 20:R285–R295. http://dx.doi.org/10.1016/j.cub.2010.01.034

Verdaasdonk, J.S., P.A. Vasquez, R.M. Barry, T. Barry, S. Goodwin, M.G. Forest, and K. Bloom. 2013. Centromere tethering confines chromosome domains. *Mol. Cell*. 52:819–831. http://dx.doi.org/10.1016/j.molcel.2013.10.021

Volkov, V.A., A.V. Zaytsev, N. Gudimchuk, P.M. Grissom, A.L. Gintsburg, F. I. Ataullakhanov, J.R. McIntosh, and E.L. Grishchuk. 2013. Long tethers provide high-force coupling of the Dam1 ring to shortening microtubules. *Proc. Natl. Acad. Sci. USA*. 110:7708–7713. http://dx.doi.org/10.1073/pnas.1305821110

Warsi, T.H., M.S. Navarro, and J. Bachant. 2008. DNA topoisomerase II is a determinant of the tensile properties of yeast centromeric chromatin and the tension checkpoint. *Mol. Biol. Cell*. 19:4421–4433. http://dx.doi.org/10.1091/mbc.E08-05-0547

Waters, J.C., R.V. Skibbens, and E.D. Salmon. 1996. Oscillating mitotic newt lung cell kinetochores are, on average, under tension and rarely push. *J. Cell Sci.* 109:2823–2831.